# THE DEPENDENCE OF RADAR TARGET DETECTABILITY ON ARRAY WEIGHTING FUNCTION

## C.M. Alabaster*, E.J. Hughes*

*Cranfield University, DCMT Shrivenham, UK. Email c.m.alabaster@cranfield.ac.uk

## Abstract

This paper assesses the dependence of target detectability in the presence of clutter on the transmitting and receiving antenna array weighting functions for airborne, medium pulse repetition frequency radar. Target detectability is best for functions which result in the lowest average sidelobe levels.

## 1 Introduction

This paper describes simulation work to assess the detectability of targets by an airborne fire control radar (FCR) operating in a medium pulse repetition frequency (PRF) mode in the presence of strong ground clutter as a function of transmitting and receiving array weighting functions. It describes the radar, antenna and clutter modelling for a system operating a 3 of 8 medium PRF schedule waveform. Medium PRF waveforms and the selection of PRFs are described in the authors' previous papers [1,2,4].

Target detectability depends on the number of PRFs in which any target is visible and on the probability of detection (Pd) in each PRF. The Pd in each PRF is determined by the signal to noise plus clutter ratio (SNCR), amongst other factors, and varies across the range and velocity (Doppler) detection space of the radar due to the ambiguous repetition of clutter across this detection space. Minimizing side lobe clutter (SLC) through the minimization of antenna sidelobe level is a design priority for such systems. This may be achieved by applying a tapered illumination function across the antenna aperture and can be implemented readily by appropriate amplitude and phase weightings of the elements of an active electronically scanned array (AESA) antenna. However, tapered illumination functions result in a reduction in main beam boresight gain together with a broadening of the main beam, both of which are further degraded when the beam is phase steered away from its mechanical boresight. Furthermore, phase steering tends to generate increased sidelobes. Thus there appears to be a conflict of interests in applying tapered illumination across an array antenna as far as target detection is concerned; on the one hand the tapered illumination reduces the sidelobe level but on the other it leads to a loss of main beam gain. Thus both clutter and target signal strengths are reduced through the use of a tapered antenna illumination or, conversely, both are maximized for a uniformly illuminated antenna. The question arises as to whether tapered illumination actually leads to increased target detectability or not in scenarios in which target detection is likely to be clutter limited (i.e. low flying, look-down).

This question has been addressed by modelling the clutter scene in an airborne FCR for various combinations of transmitting and receiving array weighting functions, azimuth and elevation steering angles, platform altitudes and probabilities of failed array elements. For each combination of conditions, target detectability is derived over the full range/velocity detection space of the radar. Comparisons between the target detectability of the various conditions are evaluated in order to determine the optimum transmitting and receiving array weighting functions.

Section 2 of this paper describes the radar, antenna and clutter modelling processes and the method by which target detectability is derived and compared. In section 3, the results are presented and discussed. Finally, section 4 draws some conclusions.

## 2 Modelling processes

### 2.1 Radar model

The radar model is intended to be representative of a modern airborne FCR. Radar parameters are summarised in Table 1.

| Parameter | Value |
|---|---|
| Frequency | 10GHz - fixed |
| PRI (=1/PRF) | 35.5, 38.5, 44.5, 49.5, 56.0, 64.5, 69.0 and 94.0 µs |
| Space charging time | 1.7ms |
| Target illumination time | 42.496 ms |
| Duty ratio | 10% (fixed) |
| Peak transmitted power | 10 kW |
| Pulse compression | Yes – variable with PRF |
| Range resolution | 75 m (0.5µs in time) - fixed |
| Doppler processing | 64 point FFT |
| Eclipsing blindness | transmitted pulse width + 0.5µs |
| Maximum range | 185 km (100 nmi) |
| Maximum velocity | 1500 ms$^{-1}$ (Doppler = 100kHz) |
| System noise figure, F | 5 dB |

Table 1: Radar Model Parameters.

It has been assumed that the radar operates on a medium PRF schedule of 8 PRFs and requires target data in a minimum of 3 PRFs for range and Doppler ambiguity resolution using the coincidence algorithm. The selection of the 8 pulse repetition intervals (PRI = 1/PRF) was made in a separate exercise as described in [1,2,4]. No main beam clutter (MBC) rejection is assumed which permits target detectability to be evaluated even in regions of strong MBC. Platform motion compensation (PMC) is applied such that the velocity of mainbeam boresight detections are ground referenced. In this way, MBC is centred at zero Doppler and at multiples of the PRF. The radar platform altitudes considered were 1000m and 5000m and the platform velocity was taken as 300 ms$^{-1}$.

## 2.2 Antenna model

A planar AESA antenna comprising 1041 elements distributed in a diamond lattice over a circular area of nominal diameter 56cm was modelled. The element spacings were nominally a half wavelength. Three possible transmitting array weighting functions were considered: Uniform, Radial Transmit Taper (RTT) and Successive Projection Transmit Nulling (SPTN) [3] and two possible receiving array weighting functions were considered: Taylor 35dB and Taylor 45dB. In addition to these 6 combinations, a seventh, that of Uniform on transmit and receive, was also considered for comparative purposes. The 7 combinations of the transmitting and receiving array weighting functions (named *patterns*) are defined in Table 2.

| *patterns* | Transmit Weighting Function | Receive Weighting Function |
|---|---|---|
| 1 | Uniform | Uniform |
| 2 | Uniform | Taylor 35 dB |
| 3 | Uniform | Taylor 45 dB |
| 4 | RTT | Taylor 35 dB |
| 5 | RTT | Taylor 45 dB |
| 6 | SPTN | Taylor 35 dB |
| 7 | SPTN | Taylor 45 dB |

Table 2: Combinations of Array Weighting Functions

The weighting function data defined the magnitude and phase of the current exciting each element. Furthermore, each element of the array was defined as having a power gain pattern which varies as the cosine of the angle off the mechanical boresight. The phase of each element was under the control of a 6 bit phase shifter. The magnitude (power) of each element was subject to a tolerance of 0.3dB (Gaussian of zero mean and σ = 0.3dB) and a phase tolerance of 2$^0$ (Gaussian of zero mean and σ = 2$^0$). The random failure of 0%, 2% and 5% of the elements was modelled by including a function which set the probability of each element having zero amplitude to 0.00, 0.02 and 0.05, respectively. Simple phase gradients were derived which provided azimuth steering angles of 0$^0$ (dead ahead), 30$^0$ and 56$^0$ and elevation steering angles of 0$^0$ (towards horizon, both platform altitudes) and 5.5$^0$ down (5000m altitude only). Therefore,

there were a total of 9 combinations of altitude, azimuth and elevation steering angles together with 3 probabilities of failed elements giving rise to 27 differing conditions for each of the 7 *patterns* i.e. 189 total simulations.

The far-field radiation pattern was derived by computing the two-dimensional Fourier transform over the array surface. Only the lower hemisphere need be derived since only this portion illuminates the ground. Furthermore, only the forward looking half-hemisphere was considered since the rear-ward looking pattern is likely to be dominated by the interaction with the radome which was outside the scope of this study. The peak main beam boresight gain for the uniform weighting function (assuming no magnitude and phase errors and zero failed elements) was normalised to 33.3dBi by an appropriate scaling factor. All other radiation diagrams were scaled by the same factor to ensure that the computed radiation diagrams represented the true effective radiated power (ERP).

The radiation pattern of the ideal antenna uniformly weighted having zero phase steering angles, no magnitude and phase errors and zero failed elements indicates a 3dB beamwidth of 3.08$^0$ and a peak sidelobe level (SLL) of 17.64dB below the main beam. Similarly, peak SLLs of -35dB and -44.5dB were obtained for the Taylor 35dB and Taylor 45dB functions, respectively. The RTT has a maximum SLL of around -20dB, whereas the SPTN has a maximum SLL of around -18dB, although its sidelobes at large angular offsets from the mainbeam boresight decay away more quickly than for the RTT. The SPTN function also gives rise to large sidelobes some 11.5$^0$ below the mainbeam boresight at a level of -23.0dB.

## 2.3 Clutter model

In modelling the clutter and noise all statistical variation has been eliminated in order to permit small changes in target detectability to be resolved. The method previously described in [1] is used. Clutter is mapped by considering the surface under the radar to be marked out by a grid along orthogonal $x$ and $y$ coordinates centred at 0,0 directly under the radar. The model steps through increments in the $x$ and $y$ coordinates in the forward half space out to the maximum range of interest. At each location the model computes the slant and ground ranges and the resolved Doppler shift along the line of sight to the radar together with the grazing angle, clutter backscatter coefficient and clutter radar cross section (RCS). The clutter RCS is computed on the basis of a clutter area equal to the square of the $x/y$ resolution which was set to 50m. The clutter backscatter coefficient (BSC) is a function of the grazing angle, $\theta_g$, which is computed for each point in the clutter modelling process. The BSC was defined as:

$$ BSC = \sigma_0 \sin(\theta_g) + \sigma_{0V}\, w \exp\left(\frac{-(90-\theta_g)}{\theta}\right) \qquad (1) $$

where $\sigma_0$ = -15 dBm$^2$ and $\sigma_{0V}$ = -5 dBm$^2$ (in linear units), and $\theta = \dfrac{-20}{\log_e\left(\sin 70^0 / A\right)}$ and $A = \dfrac{\sigma_{0V}}{\sigma_0}$

$\sigma_{0V}$ defines the BSC at normal incidence and $\sigma_0$ defines the BSC at a mid grazing angle. $w = 1$ and is the mean of a Weibull distribution appropriate to land clutter [1]. The power of the clutter returns was calculated using the following form of the radar range equation in which the clutter RCS is cascaded with the transmitting and receiving antenna gains along the line of sight to the radar by reference to the appropriate antenna radiation pattern data:

$$clutter\ power = \frac{P_T.G_T.G_R.\lambda^2.RCS_C}{64.\pi^3.R_S^4} \tag{2}$$

where    $P_T$ = peak transmitted power (= 10 kW)
       $G_T$ = transmitting antenna gain
       $G_R$ = receiving antenna gain
       $R_S$ = slant range
       $\lambda$ = wavelength = 0.03m
       $RCS_C$ = clutter RCS = BSC × *(x/y resolution)²*

The clutter power calculated from (2) was then added into the appropriate range/Doppler cell on top of the noise power and any previously calculated clutter signals. The total clutter and noise power is then stored in a two-dimensional matrix (range cell vs. Doppler cell) and displayed on a folded clutter map. A *folded* clutter map is one in which the clutter amplitude from the full detection space of the radar is folded into one ambiguous range and Doppler interval. Thus a clutter map always has 64 equal intervals in Doppler, since this is the FFT size but a variable number of range cells which is equal to the number of range cells in one PRI. A constant fixed noise power level of $k.T_0.B_n.F$ is added in to every cell of the map, in which $k$ is Boltzmann's constant = $1.38 \times 10^{-23}$ JK$^{-1}$, $T_0$ is a standard temperature of 290K, $B_n$ is the noise bandwidth = (transmitted pulse width)$^{-1}$ and $F$ is the noise figure = 3.16 (5dB). An example folded clutter map is given in Figure 1.
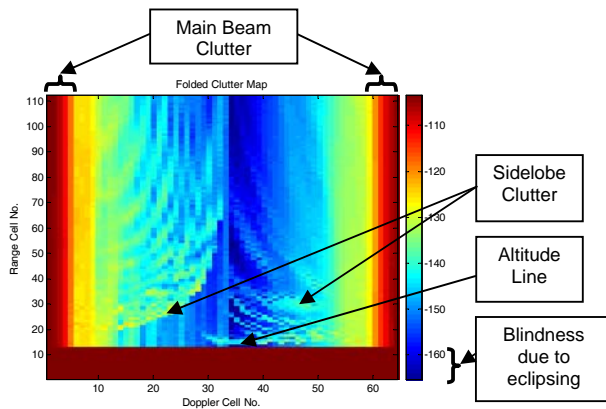


Figure 1: A Folded Clutter Map

**2.4 Target detectability**

Target detectability over the full range/Doppler detection space of interest is conveniently represented by a *detectability map* [1]. The folded clutter map of Figure 1 is replicated in range and Doppler over the full detection space of interest (i.e. 185km in range by 1500ms$^{-1}$ in velocity) due to the

repetition of data in the time and frequency domains. This results in an unfolded clutter map. Each PRF in the schedule has a similar, though different, unfolded clutter map. The probability of detection of a discrete target at any range/Doppler cell of interest depends on the number of PRFs in which the range/Doppler cell is not eclipsed and the probability of detection in each PRF, as determined by the SNCR of the cell. Blindness results from eclipsing, with no MBC blanking being assumed. A detectability map can therefore be derived over the full range and Doppler detection space of the radar and denotes the minimum target RCS required for detection at each range and Doppler cell in an appropriate number of PRFs. An example detectability map is given in Figure 2 based on a required SNCR = 0dB in at least 3 PRFs from the total of 8. Similar criteria have been used in the generation of all detectability maps used in this study. Should a more realistic SNCR of, for example, +13dB be required, one need only apply a 13dB offset to the detectability map data. In this work the benefits of different array weighting functions were derived through comparisons between detectability maps. Detectability maps are a useful means of characterizing relative performances in clutter
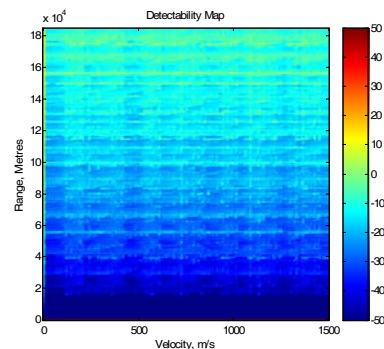


Figure 2: Detectability Map

**2.5 Evaluating target detectability**

Each of the 189 simulations results in 8 folded clutter maps; one for each PRF. However, the Doppler resolution (=*PRF/FFT_size*) and number of range cells (= *PRI/0.5µs*) differs in each of the eight. In constructing the detectability map the eight folded clutter maps are overlaid and unfolded to occupy the whole range and Doppler detection space of the radar. This requires that they be read at a common resolution which can be no finer than that of the coarsest map. Hence the resolution of the detectability map is marginally coarser than the original clutter maps. Since all detectability maps are plotted with a common resolution it is a simple exercise to compare two maps pixel by pixel since each pixel relates to a consistent range/Doppler cell.

A test strategy was developed in which the 27 detectability maps of one set of transmitting and receiving array weighting functions (corresponding to the 27 combinations of azimuth/elevation steering angles, proportion of failed elements and platform altitude) where compared with the

corresponding 27 detectability maps for each of the other six sets of transmitting and receiving array weighting functions. This progressed until all sets of transmitting and receiving array weighting functions had been compared with all the other sets. This test strategy has been found to be necessary due to the complexity of the optimization problem posed by this study. As an optimization problem, this work seeks to optimize a single objective; the detection performance of the radar, via the selection of an optimal combination of transmitting and receiving antenna weighting functions. However, the complexity arises because target detectability is quantified over several hundreds of thousands of range/Doppler cells (i.e. it is highly multi-dimensional) which must be distilled into simpler metrics. These optimization problems can typically yield several optimal solutions, collectively forming a *Pareto* surface, since the optimal solution identified by each set of comparisons may differ in each case depending on what metric is used to define target detectability and what baseline standard is adopted for each comparison. Two metrics, ($X$ and $Y$) have been derived which compare the data in pairs of detectability maps, $A$ and $B$.

**(i) Ratio of comparisons, $X$**
The algorithm runs as follows:
- Derive a logical comparison matrix for which $A>B$ and sum all its elements. (The comparison matrix consists of elements = 1 or 0 depending on whether $A>B$ or not. In summing all the elements one derives the total number of elements for which $A>B$.)
- Similarly, derive a logical comparison matrix for which $B>A$ and sum all its elements. (This derives the total number of elements for which $B>A$.)
- Derive the ratio of the two sums and express it on a decibel scale, i.e.:

$$X = 10.\log_{10}\left(\frac{\Sigma(A > B)}{\Sigma(B > A)}\right) \qquad (3)$$

If the detectability levels of $A$ are generally higher than those of $B$ then $\Sigma(A>B)$ is large and $\Sigma(B>A)$ is small, their ratio > 1 and so $X$ is a (large) positive quantity. If the reverse is true then $X$ is a (large) negative quantity. The $X$ metric gives an impression of the relative area of the range/Doppler space for which the detectability of one test is greater than the detectability of another. The $X$ metric gives no information on the margin by which one is greater than the other.

**(ii) Sum of difference comparison, $Y$**
The algorithm runs as follows:
- Derive the matrix for $A - B$. This matrix yields signed difference values.
- Cube the difference matrix element by element. This accentuates the differences and preserves their sign.
- Sum all the elements of the cubed difference matrix. This returns the net difference over the whole range/Doppler detection space.

$$Y = \Sigma(A - B)^3 \qquad (4)$$

If the detectability levels of $A$ are generally higher than those of $B$ then the $Y$ metric will be a positive number whereas, if the reverse is true, the $Y$ metric will be a negative number. The $Y$ metric gives an impression of the "aggregate" level by which the detectability of one test is greater than the detectability of another. The $Y$ metric indicates the margin of superiority but not its extent in area.

The combination of the $X$ and $Y$ metrics therefore indicate both the area extent of superiority of one detectability map over another and also on the aggregate margin of this superiority.

## 3 Results & Discussion

A series of comparisons has been made between pairs of detectability maps ($A$ and $B$) and the $X$ and $Y$ metrics of each comparison derived. Batches of 27 comparisons are made for each combination of the 7 *patterns* (Table 2) and therefore the means $\overline{X}$ and $\overline{Y}$ over the 27 comparisons have been derived. Note that the use of the mean of these metrics is not intended to imply that they have a Gaussian spread. The $\overline{X}$ results are given in Table 3 and the $\overline{Y}$ results in Table 4.

| | | A *patterns* | | | | | | |
|---|---|---|---|---|---|---|---|---|
| | | 1 | 2 | 3 | 4 | 5 | 6 | 7 |
| *B patterns* | 1 | 0 | -49.8 | -51.8 | -45.9 | -47.1 | -40.6 | -44.0 |
| | 2 | 49.8 | 0 | -7.2 | -13.7 | -15.7 | -7.7 | -11.5 |
| | 3 | 51.8 | 7.2 | 0 | -5.8 | -12.5 | -0.4 | -6.1 |
| | 4 | 45.9 | 13.7 | 5.8 | 0 | -5.5 | 5.7 | 0.4 |
| | 5 | 47.1 | 15.7 | 12.5 | 5.5 | 0 | 8.8 | 5.1 |
| | 6 | 40.6 | 7.7 | 0.4 | -5.7 | -8.8 | 0 | -6.0 |
| | 7 | 44.0 | 11.5 | 6.1 | -0.4 | -5.1 | 6.0 | 0 |

Table 3: $\overline{X}$ Results

| | | A *patterns* | | | | | | |
|---|---|---|---|---|---|---|---|---|
| | | 1 | 2 | 3 | 4 | 5 | 6 | 7 |
| *B patterns* | 1 | 0 | -3e32 | -4e32 | -5e32 | -5e32 | -6e32 | -6e32 |
| | 2 | 3e32 | 0 | -3e29 | -6.e29 | -2e30 | -3e30 | -5e30 |
| | 3 | 4e32 | 3e29 | 0 | -3e27 | -2e29 | -4e29 | -1e30 |
| | 4 | 5e32 | 6e29 | 3e27 | 0 | -9e28 | -3e29 | -8e29 |
| | 5 | 5e32 | 2e30 | 2e29 | 9e28 | 0 | -2e28 | -1e29 |
| | 6 | 6e32 | 3e30 | 4e29 | 3e29 | 2e28 | 0 | -3e28 |
| | 7 | 6e32 | 5e30 | 1e30 | 8e29 | 1e29 | 3e28 | 0 |

Table 4: $\overline{Y}$ Results

The rank order of the *B_patterns* from highest $\overline{Y}$ (best target detectability) to lowest $\overline{Y}$ (worst target detectability) for all seven sets of results is consistently: 7, 6, 5, 4, 3, 2, 1. The consistency of this result is believed to be due to the simple arithmetic expression for $Y$. The rank order of the *B_patterns* for the $\overline{X}$ results is slightly inconsistent but, in general, the highest $\overline{X}$ (best target detectability) is obtained for

$B\_patterns$ = 5 and the lowest $\overline{X}$ (worst target detectability) is consistently obtained for $B\_patterns$ = 1. The small degree of inconsistency in the rank order of the *patterns* for the $\overline{X}$ results is believed to be due to the non-arithmetical nature of the expression for $\overline{X}$ plus the fact that the baseline $A\_patterns$ = 1 is very distant from the better solutions. If one sums the $\overline{X}$ results over the seven sets of results one obtains the rank order of the *patterns* from best target detectability to worst target detectability of: 5, 4, 7, 3, 6, 2, 1.

The preferred solution depends on the metric used to quantify target detectability and the baseline against which comparisons are made. This is a typical dilemma associated with optimisation problems whose optimisation goal has high dimensionality and there is as yet no known metric which avoids the inconsistent behaviour observed here. One method to arrive at an optimum solution based on equal weightings of the $X$ and $Y$ results may be to award points to each of the *patterns* based on the rank order of their seven sets of $\overline{X}$ and $\overline{Y}$ results. The following scoring method is proposed here: 7 points are awarded for a first place in the rank order, 6 points for second place, 5 points for third and so on down to one point for a seventh place finish. Since also:

$$\text{maximum} \sum \overline{X}\_\text{points} = \text{maximum} \sum \overline{Y}\_\text{points} = 49,$$

each *patterns* has an associated distance from the best possible solution given by:

$$\text{DISTANCE} = \sqrt{\left(49 - \sum \overline{X}\_\text{points}\right)^2 + \left(49 - \sum \overline{Y}\_\text{points}\right)^2} \qquad (5)$$

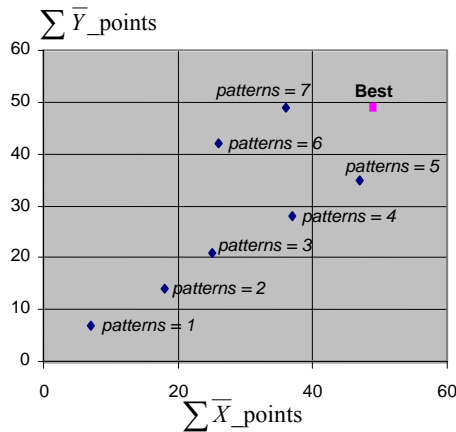The points are displayed in Figure 3.



Figure 3: Points Positions of Solutions

The ascending rank order of DISTANCE determines the rank order of the solutions defined by *patterns*. The results of the points scoring are (from best to worst): 7, 5, 6, 4, 3, 2 and 1. From Figure 3 it is evident that *patterns* = 5 and 7 are almost equal solutions which fall on a Pareto surface i.e. no one solution is better on both metrics simultaneously. However, of the two, *patterns* = 7 offers the slightly better target detectability. It may be noted that the better target detectability is generally obtained for the Taylor 45dB

weighting function to be applied to the receiving array over the corresponding Taylor 35dB function. The worst $X$ and $Y$ results were consistently obtained for *patterns* = 1, indeed all solutions which entail the transmission using the Uniform illumination function exhibit poor target detectability.

## 4 Conclusions

Clearly, the differing metrics which one may use to quantify target detectability result in differing solutions with very little to chose between the best of them. However, by combining the means of both the $X$ and $Y$ metrics in a points scoring system the best overall solution was identified as being the combination of the SPTN function on transmission and the Taylor 45dB function on reception. This was very closely followed by the combination of the RTT function on transmission and the Taylor 45dB function on reception. The overall preference for the former may well be due to its lower average sidelobe levels on transmission. Nevertheless, it ought to be stressed that the margins between these two cases are very small and may very well be masked by realistic statistical variations in noise, clutter and target RCS. It may also be worth noting that the RTT function results in an effective radiated power (ERP) some 0.6dB higher than that of the SPTN function and so enjoys a small advantage in detection performance in noise limited cases. Furthermore, the RTT function (and its resulting beam pattern) is circularly symmetrical and so remains constant irrespective of the platform roll angle. The worst target detection performance was obtained when using the Uniform illumination function on the transmitting array. Indeed the test case of the Uniform function on both transmission and reception was found by both metrics to yield the worst target detection capability by a large margin.

## Acknowledgements

## References

[1]  C. M. Alabaster & E. J. Hughes. "The Design of Medium PRF Radar Schedules For Optimum Detectability in Diverse Clutter Scenes" *Proc. IEEE Waveform Diversity & Design*, Lihue, Kaua'i, HI, USA, 22nd – 27th January 2006.

[2]  C.M. Alabaster, E.J. Hughes & J.H. Matthew. "Medium PRF radar PRF Selection Using Evolutionary Algorithms", *IEEE Trans. Aerospace and Electronic Systems*, **vol. 39, no. 3**, pp. 990-1001, July 2003.

[3]  I. M. Mellor, F. J. Adams. "Benefits of Transmit Beam Pattern Synthesis for Airborne Phased Array Radar", *Proc. IRS 2005,* Berlin, Germany, 6 – 8 Sept. 2005.

[4]  D. A. Wiley, S. M. Parry, C.M. Alabaster and E. J. Hughes. "Performance Comparison of PRF Schedules for Medium PRF Radar", *IEEE Trans. Aerospace and Electronic Systems*. **vol. 42, no. 2**, Apr 2006, pp 601-611.